ADVANCED FUNCTIONAL MATERIALS
www.afm-journal.de

Two-Dimensional Assembly of Symmetric Colloidal Dimers under Electric Fields

*Fuduo Ma, Sijia Wang, Lois Smith, and Ning Wu**

Like atoms and molecules with directional interactions, anisotropic particles could potentially assemble into a much wider range of crystalline arrays and meso-structures than spherical particles with isotropic interactions. In this paper, the electric-field directed assembly of geometrically anisotropic particles–colloidal dimers is studied. Rich phase behavior and different assembly regimes are found, primarily arising from the broken radial symmetry in particles. The orientations of individual dimers depend on the frequency of the electric field, the ramping direction of frequency, and the salt concentration. The competition and balance between the hydrodynamic, electric, and Brownian torques determine the orientation of individual particles, while the competition between the electrohydrodynamic force and dipolar interaction determines the aggregation of aligned particles at a given experimental condition. The field distribution near the electrode is critical to understand the orientation and assembly behavior of colloidal dimers on a conducting substrate. This study also demonstrates the effectiveness, the reversibility, and potential opportunity of applying electric field to control the orientation and direct the assembly of non-spherical particles. In particular, two dimensional close-packed crystals of perpendicularly aligned dimers are obtained, which shows promise in fabricating 3D photonic crystals based on dimer-like colloids and field-directed display.

1. Introduction

Bottom-up assembly of atoms and molecules into well-defined structures is a natural but complex process through which materials form. Our current understanding and ability to control matter at the atomic and molecular levels are limited due to the difficulty in observing and characterizing the *in situ* dynamics of the assembly process at sufficiently small length and time scales. Studies of micron-sized particles with isotropic interactions (as artificial atoms) have significantly enriched our fundamental understandings in crystallization, phase transitions, glass formation, etc. The types of structures that isotropic particles can form are nevertheless very limited due to the lack of directional interactions between particles. Close-packed crystals such as the face-centered cubic or the hexagonal close packing are often observed. Recently, particles with anisotropic properties in geometry, chemical composition, or surface functionality have been envisioned as more faithful building blocks for mimicking atoms and molecules.[1–5] By tuning the anisotropic interactions, one could be able to visualize, understand, and manipulate the dynamic assembly pathways of anisotropic particles into diversified types of crystalline and non-crystalline structures, similar to what have been observed in the molecular world. Moreover, anisotropic particles, as novel and complex building blocks, could be used to construct artificial crystals with exotic properties, such as photonic crystals with robust and complete band gaps[6,7] and plasmonic structures for light concentration.[8,9]

The simplest form of anisotropic particles is the so-called Janus spheres,[10,11] in which surface chemistry is different on opposite sides of the particle, although geometrically the particles are still isotropic. Examples of geometrically anisotropic particles include non-spherical particles, such as ellipsoids,[12] rods,[13] and clusters of spheres (colloidal dimers, tetramers, etc).[14] Among different types of anisotropic particles, the polymeric colloidal dimers are of particular interest. They can be bulk-synthesized with high monodispersity in size.[15–18] The differences in surface functionalities and geometric sizes[15] between two lobes can be tuned conveniently. Therefore, the colloidal dimer is a good candidate for systematic investigation of the impacts of individual type of anisotropies on self- and directed assembly. Moreover, numerical simulations[6,19] have shown that dimers could be potential building blocks for creating photonic crystals with diamond-like lattices, which exhibit superior and robust photonic properties. This further motivates our current study in the electric-field driven assembly of colloidal dimers.

While many theoretical and numerical models have been developed for various imaginable types of anisotropic particles, the experimental investigations lag behind primarily due to the difficulty of making particles with well-controlled anisotropy in high yield. Despite this obstacle, recent experimental studies on the self-[20–22] and field-directed assembly[7,23–27] of

F. Ma, S. Wang, Prof. N. Wu
Department of Chemical Engineering
Colorado School of Mines
Golden, CO 80401, USA
E-mail: ningwu@mines.edu
L. Smith
Department of Physics
University of Colorado–Boulder
Boulder, CO 80301, USA

DOI: 10.1002/adfm.201200649

anisotropic particles have shown much more diversified types of structures and significant advantages over isotropic particles. In particular, three-dimensional assembly of symmetric dumbbell particles of silica[25] and polystyrene[26] have been studied under electric fields very recently. The assemblies were, however, mainly driven by the induced dipolar interaction at high frequencies, which limit the orientational control of the non-spherical particles. Additional long-range force, such as the electrohydrodynamic (EHD) interaction, has been shown very effective in assembling spherical particles.[28–31] But the control of orientation and assembly of non-spherical particles by the EHD interaction has not been reported yet. Systematic investigations of the influences of geometric, chemical, and physical anisotropies on assembly are far from sufficient to explore the full potentials of anisotropic particles. Unconventional materials with exotic properties assembled by anisotropic particles are yet to be demonstrated.

In this paper, we will show interesting phenomena during low-frequency electric-field directed assembly on a conducting substrate. In additional to the induced dipolar interaction, the electrohydrodynamic interaction is important for both orientational control and the assembly of colloidal dimers. Although colloidal dimer is a simple system that deviates from isotropic sphere by breaking the radial symmetry, we have observed rich phase behavior and different assembly regimes primarily due to the geometric anisotropy. The orientations of individual dimers depend on the frequency of the electric field, the ramping direction of the frequency, and the salt concentration. The competition and balance between the hydrodynamic and electric interactions determine both the orientation and aggregation of colloidal dimers. We have also obtained two dimensional close-packed crystals of aligned dimers, which shows promise in fabricating 3D photonic crystals based on anisotropic particles.

2. Results and Discussion

2.1. Experimental Setup

Figure 1a shows a typical SEM image of the polystyrene dimers used in the experiments. They are synthesized based on a modified strategy (see the experimental section) of the "seeded emulsion polymerization".[15,16,18] Both lobes are of similar sizes (within 3% difference). The short axis of the dumbbell is ~ 1.5 μm. Although dumbbells of smaller or bigger sizes can be readily synthesized, we focus on the micron-size range in this paper for convenient *in situ* observations under optical microscope and minimization of the gravitational effect. The ratio $L_1/2L_2$ is a key parameter to characterize the degree of overlap between two lobes (1 for tangentially connected dimers). Particles used in our experiments typically possess $L_1/2L_2$ ~ 0.8–0.9. We have also tried to balance the amount of negative charges on both lobes through controlled addition of ionic co-monomers (sodium styrene sulfonate) during the synthesis of CPS and dimers. Zeta potential measurement in different salt concentrations (potassium chloride KCl) is shown in Figure 1b. As expected, it decreases with decreasing salt concentrations. The inset of Figure 1b shows zeta potential measurement at

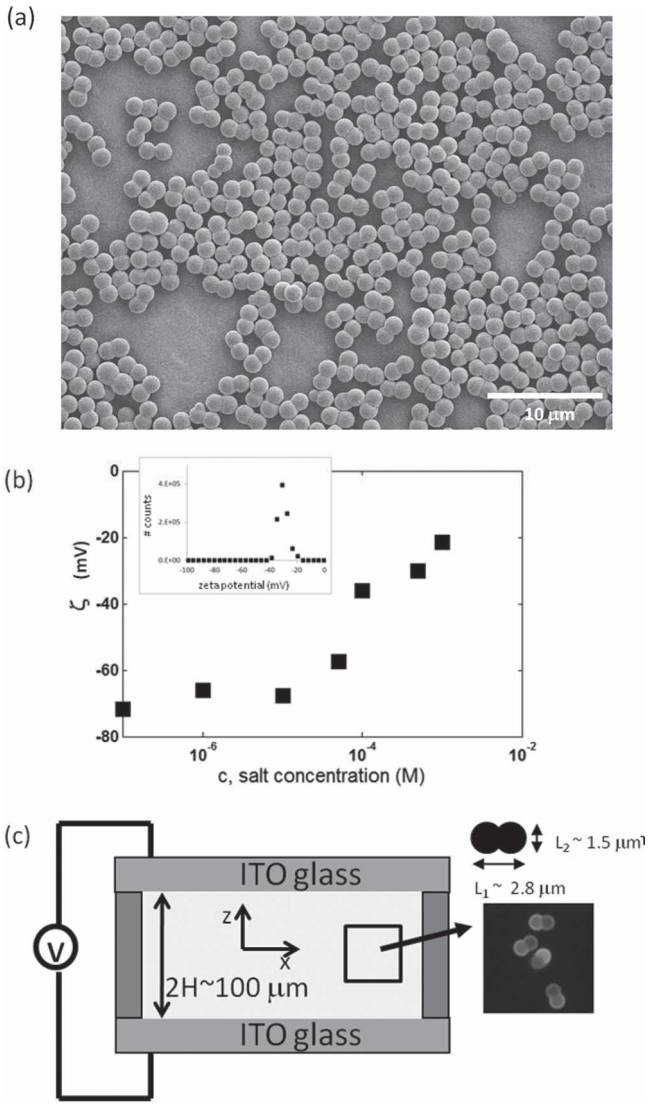

Figure 1. (a) The SEM image of colloidal dimers synthesized and used in our experiments. (b) Change of zeta potentials with salt concentrations. Inset: the statistical distribution of zeta potentials in one typical measurement (10^{-4} M KCl). (c) The experimental setup of the electric-field driven assembly. The fluoresecent image is obtained after coating the dimers with positively charged dye, rhodamine 6G.

10^{-4} M KCl. The sharp peak confirms the uniform distribution of charges among different colloidal dumbbells. We have also coated positively charge fluorescent dyes (rhodamine 6G) on (negatively charged) dimers. As shown in Figure 1c, the contrast in the intensity of fluorescence indicates weakly asymmetric distribution of surface charges on the same dimer. Therefore, the colloidal dimers used in this study are symmetric dumbbells with identical geometric sizes and approximately similar amount of surface charges on both lobes. Although it represents a simple deviation from the conventional colloidal spheres, understanding the assembly behavior of this type of dimers will form the baseline for comparison with latter studies of more complex forms of dimers.

A cross-section view of our experimental setup is shown in Figure 1c. A thin film of colloidal suspension is sandwiched between two pieces of ITO (indium-tin-oxide) glasses with insulating spacers to control the separation between two electrodes. Real time observations are performed on an inverted bright-field microscope with a focus on the bottom substrate. An external voltage bias (DC or AC) is maintained between two ITO glasses. Therefore the direction of applied field is perpendicular to the plane of conducting substrates. Various amounts of salt (KCl) are added in water to adjust the Debye length and zeta potentials.

2.2. Theoretical Background

In this section, we first review the possible forces involved in the two-dimensional assembly of spherical particles under the influence of an electric field, and then extend our discussion to non-spherical colloids. The applied electric field has the form $\tilde{E} = Ee^{i\omega t}$, where ω represents the frequency. This field, in general, induces a dipole moment p on the colloids, which is proportional to the applied electric field, i.e., $p = \alpha \tilde{E}$. The proportional constant α is the polarizability of the particle, whose magnitude depends on the permittivities and bulk conductivities of both particle and solvent, as well as the surface conductivity of the particle.[32] Particles i and j on a flat substrate experience an induced dipole-dipole repulsion if their mutual alignment is perpendicular to the external field

$$F_d = \frac{3\mathrm{Re}\left(\alpha_i \alpha_j^*\right) E^2}{4\pi \varepsilon_s \varepsilon_0 r_{ij}^4} \quad (1)$$

where $\mathrm{Re}(\cdot)$ denotes the real part of a complex number, α^* is the complex conjugate, ε_s is the dielectric constant of the solvent, ε_0 is the permittivity of vacuum, and r_{ij} is the center-to-center distance between particles i and j. Although particles repel each other due to the dipolar interaction, they still can surprisingly aggregate and form 2D crystals on the electrode under both DC and AC fields.[28,29] Active research in understanding the assembly mechanisms have been performed during the past decade. In general, the aggregation of similarly charged particles under a DC field is mainly caused by the equilibrium-charge electroosmotic (ECEO) flow along the surface of the particles, which brings nearby particles together and generates an apparent attraction between two particles. When the attraction is strong enough to overcome the dipolar repulsion or double layer interaction between particles, close-packed crystals can be formed. The ECEO velocity of solvent is[31]

$$u_{ECEO} \propto \frac{\varepsilon_s \varepsilon_0 \zeta E}{\mu} \quad (2)$$

where μ is the viscosity of solvent and ζ is the particle's zeta potential. If we assume the particle velocity u_p is proportional to the velocity of water, we can obtain an estimation of the "hydrodynamic" attraction based on Stoke's law

$$F_a = 6\pi \mu u_p a \sim \beta 6\pi \varepsilon_s \varepsilon_0 \zeta Ea \quad (3)$$

where a is radius of the particle and $\beta \sim 0.01$ is the emperical factor that relates μ_p to μ_{ECEO}.[33]

The aggregation of spherical colloids under an AC field is more complicated and several different mechanisms have been proposed. For $\omega > 10^3$ Hz, Ristenpart et al.[34] proposed that the electric field induces excess surface charges within the polarization layer of the electrode. In addition, the particle on the substrate perturbs the originally normal electric field and an tangential component along the electrode is generated. The tangential field acts on the induced surface charges and generates an attractive or repulsive electroosmotic flow, depending on the (real part of) polarizability of the particle. Therefore, this mechanism is called the induced-charge electroosmotic (ICEO) aggregation. The ICEO velocity[30,34] is proportional to E^2, as compared with the E^1 dependence in ECEO. For $\omega < 10^3$ Hz, both ECEO and ICEO mechanisms could be important.[31] A puzzling observation is that the tendency of particles to aggregate or separate depends on the types of electrolytes in water.[35] A series of models have been proposed,[31,36] although full understanding is still to be elucidated.

We expect the above forces could also be exerted on non-spherical particles under the field-driven assembly. Since the ICEO flow is originated from the induced surface charges close to the electrode, it is the strongest near the substrate and becomes weaker further away. Therefore, a hydrodynamic torque could be possibly generated on a particle that is close to the substrate. Although this torque might be hard to detect on spherical particles, it could be clearly observed on non-spherical particles if it is strong enough to cause their rotations. In addition, non-spherical particles will typically be subject to an electric torque which could also rotate the particle. The equilibrium orientation of a non-spherical particle due to the electric torque is determined by the signs of torques in x, y, and z axes.[32] Energetically, the non-spherical particles will align one of its principle axes with the applied field to minimize the field-dipole interaction energy U_{FD}. For symmetric dumbbells, we will approximate them as ellipsoids for simplicity. U_{FD} can then be expressed[37]

$$U_{FD} = -\frac{1}{2}\mathrm{Re}\left(\alpha_{\parallel} - \alpha_{\perp}\right) E^2 \cos^2\theta \quad (4)$$

where $\alpha = 4\pi\varepsilon_0\varepsilon_s ab^2 K$ and $\alpha = 4\pi\varepsilon_0\varepsilon_s ab^2 K_{\parallel}$ are the anisotropic polarizabilities when particles are aligned parallel or perpendicular to the applied field, respectively.[32] a and b are the semi-axes of the ellipsoids, and θ is the angle between dumbbell's long axis and the field direction. $K_{\parallel}$ and $K_{\perp}$ can be expressed[32]

$$K_{\parallel(\perp)} = \frac{\varepsilon_p^* - \varepsilon_s^*}{3\left[\varepsilon_s^* + \left(\varepsilon_p^* - \varepsilon_s^*\right) L_{\parallel(\perp)}\right]} \quad (5)$$

where ε_p^* and ε_s^* are the complex permittivities of the particle and solvent: $\varepsilon^*_p = \varepsilon_0\varepsilon_p + \sigma_p/i\omega$ and $\varepsilon^*_s = \varepsilon_0\varepsilon_s + \sigma_s/i\omega$. $L_{\parallel(\perp)}$ is a parameter that only depends on the geometric dimensions of the particle (a and b).[32] In principle, $K_{\parallel(\perp)}$ is a complex function of the frequency, particle geometry, and electric properties of both particles and solvent. Analytical expressions for ellipsoids are only available for Maxwell–Wagner-O'Konski dispersion at very high frequencies (>1 MHz).[37] At the low frequency regime (<10 kHz), additional polarization of particles can arise from the Dukhin–Shilov dispersion of the double layer, which has been studied extensively for spherical particles.[38] However,

little is known for non-spherical particles in this low frequency regime.

Since the applied field in our experiments is perpendicular to the substrate, a standing dimer aligns its major axis parallel to the electric field ($\theta = 0$), while a lying dimer aligns its major axis perpendicularly to the field ($\theta = \pi/2$). According to Equation (4), the electric torque will force the dumbbell to stand (i.e., parallel to the field) if $\mathrm{Re}\left(K_{\parallel} - K_{\perp}\right)$ is greater than zero. Colloidal particles of micron-sizes would also undergo Brownian motions in liquid. Therefore, the orientation of a non-spherical particle in electric-field driven assembly is determined by the competition between the hydrodynamic, electric, and Brownian torques. When the particle is in bulk or on the substrate but far away from the assembled structures, the hydrodynamic torque is negligible. The electric torque will then compete with thermal fluctuations to orient the particle. When the particle is attracted to the assembled structures along the substrate, hydrodynamic torque could be strong enough to compete with the electric torque and Brownian motion. The delicate balance between those three torques results in the rich behavior of colloidal dimers during E-field driven assembly, as evidenced in this paper. Due to the small difference in density between water and polystyrene, the effective gravitational energy difference between "standing" and "lying" dumbbells in our experiments is much less than kT. Therefore, gravity plays little role in affecting the orientation of a dumbbell in our experiments.

2.3. Assembly Under the DC Field

We first investigate the assembly of colloidal dumbbells under a DC electric field where the bottom substrate is positively polarized. Before applying voltages, colloidal dumbbells undergo Brownian motions within the gap between two electrodes. As the voltage is increased, negatively-charged particles are attracted to the bottom substrate from the bulk due to electrophoretic motions. They, however, remain dispersed and rotate freely once arriving on the substrate. The dumbbells will start to assemble quickly when the applied voltage exceeds ~2.4 V, independent of the gap distance between two electrodes. A typical aggregate formed by colloidal dumbbells is shown in **Figure 2**a. All particles lie on the substrate and locally ordered structures can be observed. If the polarity on the substrate is reversed, the aggregate will disassemble. This observation is consistent with the observations in DC-field assembly of spherical particles, where the aggregation is mainly caused by equilibrium-charge electroosmotic flow surrounding the particles and on the substrate. According to Equation 2, the electroosmotic velocity is proportional to the zeta potential ζ and the external field E. Since the measured zeta potential of the dumbbell-shape particles decreases with increasing salt concentration (Figure 1b), the assembly velocity should become smaller at higher salt concentrations. This is confirmed by our observation that the tendency to form close-packed aggregate becomes weaker when the salt concentration is increased. No assembly was observed with a salt concentration of 10^{-3}M, where $\zeta \sim -21mV$. As a comparison, $\zeta \sim -66mV$ when the salt concentration is 10^{-6}M.

Unlike crystals formed by spherical particles, the amorphous aggregate in Figure 2a is due to the broken radial symmetry of the dumbbell particles. Since both lobes are made of the same material with similar amount of surface charges, there are no preferred directional interactions between dimers. The electroosmotic flow which causes the aggregation, however, renders particles to align locally. We can quantify the 2D alignment of particles by calculating the order parameter S

$$S(r) = \frac{1}{N}\sum_{i=1}^{N}\cos 2\theta_i \tag{6}$$

where θ_i represents the angle between a single dumbbell and the average direction of all N number of dumbbells (the arrow in Figure 2b) within a pre-defined space of radius r. The order parameter $S(r)$ is evaluated within concentric circles of radius r varying from 2 μm to 64 μm. Three representative circles with increasing r are illustrated in Figure 2a. S characterizes the degree of alignment among non-spherical particles: 0 for complete randomness and 1 for perfect alignment. Figure 2b shows $S(r)$ at two different voltages. Both curves indicate that the particles are aligned locally ($r < 10$ μm) while the aggregate loses its long range order quickly as the domain size increases.

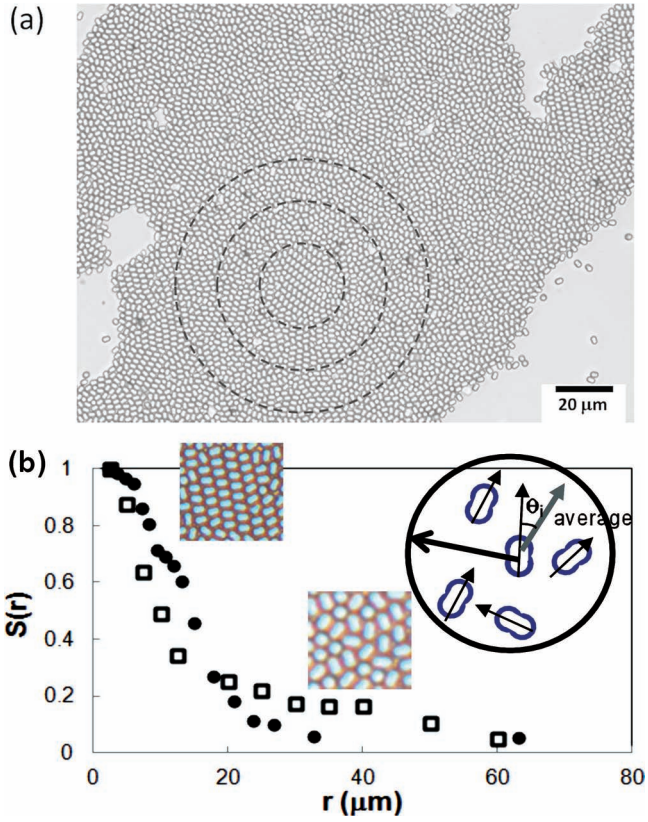

Figure 2. (a) An optical microscopy image of the dumbbells' aggregate under a DC field (2.4 V across a 100 μm gap). The KCl concentration is 10^{-6} M. Three representative circles illustrate the paths for the analysis of the order parameter $S(r)$. (b) The calculated two-dimensional order parameters at two different voltages demonstrate the short-range order and long-range disorder in the aggregate. Solid circle: 2.4 V and hollow square: 2.8V.

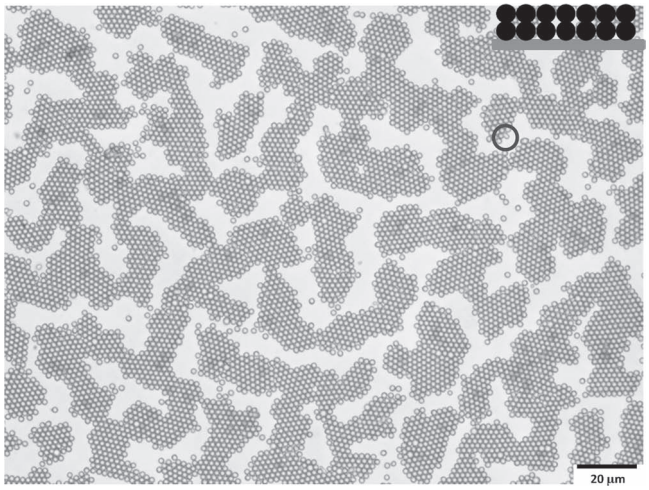

Figure 3. The crystal of standing dimers under an AC field (11 V, 6 k Hz). The only lying dimer within the field of view is highlighted with a circle.

Increasing the applied voltage does not improve the alignment of dimers over long distance. We observe that the stronger electroosmotic flow suppresses Brownian motion which can reorient misaligned dimers.

2.4. Assembly Under the AC Field

Figure 3 shows the top view of crystals formed by standing dimers under an AC field. Particles are aligned perpendicular to the substrate (parallel to the field) and form close-packed crystals. The crystal is nearly perfect and the only lying dimer in the field of view is highlighted with a circle. This is achieved by tuning frequencies under a constant voltage. We first tuned the frequency to ~10^4 Hz, where the electric torque is strong enough to align dimers parallel to the applied field. We then slowly reduce the frequency into the regime where the electroosmotic flow is strong enough to induce the assembly of those standing dimers. The assembly/disassembly process is reversible and frequency dependent, as demonstrated in the Supporting Information movie 1.

We have also investigated the phase behavior of colloidal dumbbells at different field strengths, frequencies, and salt concentrations. We find that "phases" and "phase boundaries" depend weakly on the field strength for a given salt concentration, but are sensitive to the frequency. The "phase diagram" in 10^{-3} M KCl solution is plotted in **Figure 4**. The arrows indicate the direction of frequency ramp. When there is no external field, dimer particles in the bulk rotate evenly in all directions. But once they approach the substrate, most of them adopt lying orientations although they still can rotate freely in two dimensions. This could be due to an attraction between dimer particles and the corresponding image charges on the other side of the conducting substrate. When the field is turned on, we have observed four different types of aggregation processes. Starting from a low frequency along path 1, we observe a regime where individual lying dimers approach each other and aggregate. They, however, change their orientations into standing positions

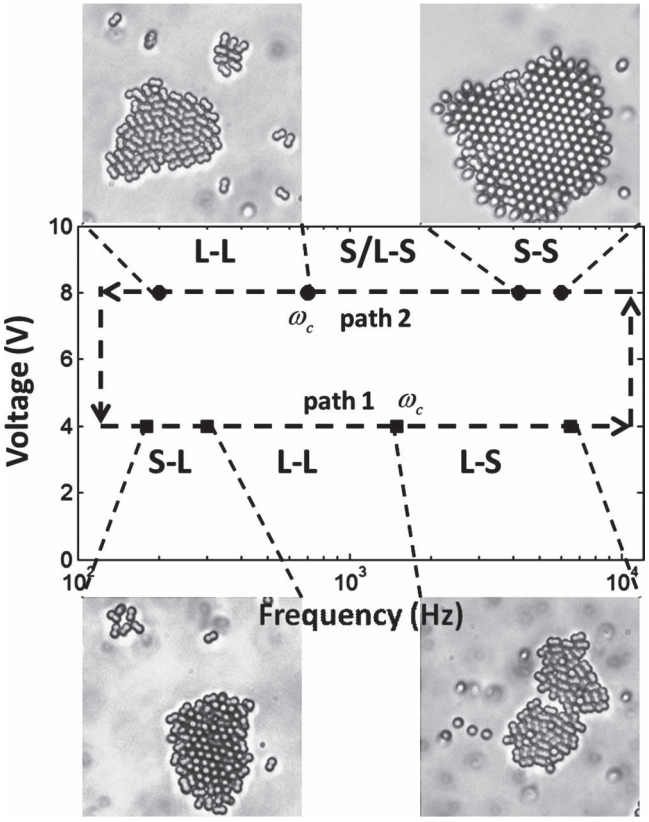

Figure 4. The phase diagram of dimers' assembly under an AC field with 10^{-3} M KCl. Varying the field strength does not change the phases and phase boundaries qualitatively. The arrows indicate the direction of the frequency change. Phase boundaries are represented by the solid squares and circles. The grey square and circle mark the critical frequencies ω_c where the dimer particles (either in the bulk or on the substrate but far away from the aggregate) start to change their orientations: lying -> standing along path 1 and standing -> lying along path 2. Different phases are represented by two letters S and L, where S means "standing" and L means "lying" on the substrate. The letter before the hyphen indicates the orientation of particles within the aggregate while the letter after the hyphen represents the orientation of particles far away from the aggregate but near the substrate. For example, S-L means that the particles stand in the aggregate but lie down if they are far away from the aggregate.

within the aggregate, as shown in the Supporting Information movie 2. We name this phase "S-L", in which the first letter S represents standing dimers within the aggregate and the second letter L stands for lying dimers far away from the aggregate. As the frequency increases, the particles in the aggregate change into lying orientations, which results in the "L-L" phase (see Supporting Information movie 3). The morphology of the "L-L" phase is very similar to the aggregate observed under DC field although the mechanism of aggregation is diffserent. Within this intermediate frequency range, the tangential field (arising from the perturbation of the normal electric field by the particle on the electrode) acts on the induced-charges within the polarization layer of the electrode and generates an electroosmotic (ICEO) flow along the substrate, which causes the aggregation of particles. Above a critical frequency (~1.5 kHz, the square ω_c in Figure 4), the free dumbbells far away from the aggregate

start to orient themselves perpendicular to the substrate (parallel to the electric field), primarily because the electric torque is strong enough above this critical frequency. The particles within the assembly are still lying down. Therefore, the "L-S" phase is observed. When standing dimers approach the aggregate, they, however, change into the lying orientations (see Supporting Information movie 4). This is because the ICEO flow is non-uniform in the vertical direction: being stronger near the substrate and weaker further away. This flow can generate a hydrodynamic torque that competes with the electric torque and re-orients the standing dimers if it is stronger. Within the L-S regime but near its high frequency border, we find that the tendency of re-orienting an incoming standing dimer becomes much weaker. Loosely packed S-S phase could be observed. This is because the ICEO flow is weak in the high frequency regime and is insufficient to realign a standing dimer horizontally, as we will demonstrate in section 2.5. As the frequency is further increased, the particles finally disassembles, because the strength of attraction due to ICEO is inversely proportional to frequency (for spherical particles[30]). It is no longer sufficient to overcome the dipole-dipole repulsion between particles at high frequencies. We confirm that the above "phases" can be achieved by a pulse supply of the electric field to the appropriate frequency regime from well dispersed samples that has been annealed under no electric field for long time (to remove "memory" of the sample).

As we move along path 2, where the frequency is decreased, we first observe the "S-S" phase. All individual dimers stand at high frequencies and they start to aggregate and form "standing crystals" when the ICEO flow is strong enough, i.e., below ~ 6000 Hz. This is the similar regime where we obtain Figure 3. As the frequency is further decreased, standing dimers start to lie down when they join in the pre-formed aggregate, so the resulting aggregate consists of a mixture of "S" and "L" dimers, i.e., the phase "S/L-S". This is because ICEO flow becomes stronger as the frequency decreases. It generates a strong hydrodynamic torque that dominates over the electric torque to re-orient the standing dimers into lying positions. Since the ICEO flow is the strongest near the periphery of the aggregate, standing dimers will change into lying orientations only when they are close to the aggregate. Individual dimers far away from the aggregate still assume the standing orientations because of weak electroosmotic flow locally. With further decrease in frequency, the electric torque also becomes weaker until it cannot sustain the standing orientation for individual dimers, marked by the grey circle ω_c along path 2. Below this critical frequency, both free dimers and aggregating dimers lie on the substrate, therefore, the "L-L" phase is observed again. We emphasize that the applied field strength has little effect on the positions of "phase boundaries" shown in Figure 4, as long as it is strong enough (≥2 V across the 100 μm gap). Frequency, however, plays the major role in determining the orientation and aggregation of dimers, a vital observation that deserves further discussions in section 2.5.

We have also explored the phase diagram for different salt concentrations, as depicted in **Figure 5**. The arrow indicates the direction of the frequency change. The profile of Figure 5 is similar under different field strengths which indicates various forces involved in the assembly process scale similarly

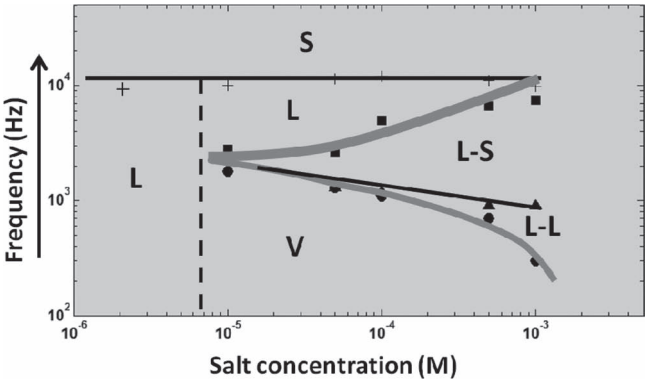

Figure 5. The phase diagram for assembly of dimers under different frequencies and salt concentrations. Different phases are represented by "L", separated lying dimers; "S", separated standing dimers; "V", vortices; "L-L", and "L-S".

with the field strength. In general, dumbbells maintain separated and standing orientation on the substrate above ~10^4 Hz - the "S" phase beyond the top line. No close-packed assembly is observed at all frequencies if the salt concentration is below 10^{-5} M. Two thicker lines define the assembly and disassembly frequencies between which stable and two-dimensional close-packed aggregates can be observed. This assembly regime is further divided into "L-L" and "L-S" phases, separated by a thin line (the critical frequencies ~10^3 Hz) at which individual particles change from the lying to standing orientation when they are far from the aggregate or in the bulk. The particles are, however, still lying on the substrate when they approach and join in the aggregate because of the hydrodynamic torque induced by ICEO flow. Beyond the disassembly line (between L and L-S), aggregated particles start to separate from each other. It indicates that the attractive ICEO flow is insufficient to balance the repulsive dipole-dipole interactions. The hydrodynamic torque is, however, still strong enough to overcome the electric torque so the dumbbells disassembled from the aggregate still maintain lying orientations until the top line is passed (where ICEO is negligible). At low frequencies, "vortices" can be observed presumably due to the Faraday current.[39]

2.5. Orientation and Aggregation of Individual Colloidal Dimers

We have found rich behavior in the electric-field driven assembly of colloidal dimers. Most noticeably, both the orientation and aggregation of individual dimers highly depend on frequency and salt concentration, under the same applied field strength. In this section, we will explain our key observations, based on the idea that the real electric field near the electrode is non-uniform and can be very different from the applied field, depending on both frequency and salt concentration. The electric field distribution in an aqueous solution across two electrodes was proposed by Hollingsworth and Saville[40] in the following expression:

$$E(\omega) = \frac{\Delta\phi}{2H} e^{i\omega t} \left[\frac{\gamma \cosh(\gamma z/H) \csc h\gamma + i\gamma\upsilon^2 \coth\gamma}{1 + i\gamma\upsilon^2 \coth\gamma} \right] \quad (7)$$

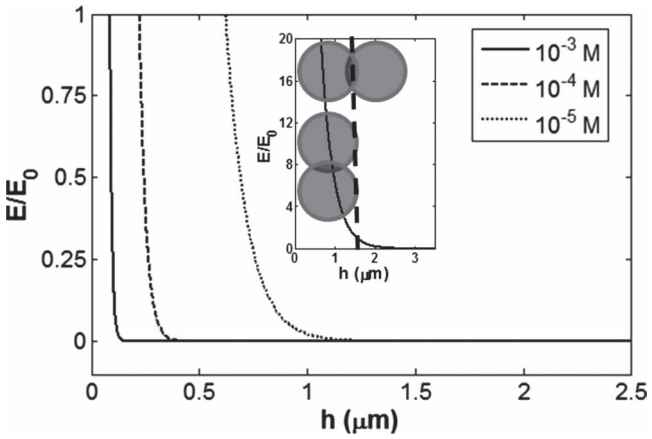

Figure 6. The distribution of DC electric field near an electrode at three different salt concentrations. The field is normalized by the "apparently" applied field calculated based on the applied voltage and the gap ($E_0 = \Delta\varphi/2H$). h is the distance from the bottom electrode. Inset: the field distribution at 10^{-6} M KCl on lying and standing dimer near the electrode. The dotted line indicates the distance from the electrode within which E/E_0 is greater than one.

where $\gamma = [(\kappa H)^2 + i\omega H^2/D]^{1/2}$, $\upsilon = (\omega/D)^{1/2}/\kappa$, $\Delta\varphi$ is the applied voltage, κ is the Debye length, D is the diffusivity of ions, and $E_0 = (\Delta\varphi/2H)ei^{\omega}t$ is the "apparent" field.

2.5.1. Assembly Under DC Field

Taking the limit $\omega \to 0$, Equation (7) can be further simplified:

$$E(\omega \to 0) = \frac{\Delta\phi}{2H}\frac{\kappa H\cosh(\kappa z)}{\sinh(\kappa H)} = \frac{\Delta\phi}{2\kappa^{-1}}\frac{\cosh(\kappa z)}{\sinh(\kappa H)} \quad (8)$$

Several important characteristics of the DC field can be revealed from Equation 8. First, most of the applied voltage drops within the double layer. Compared with the apparent field strength $E_0 \sim \Delta\phi/2H$, the actual field amplifies significantly within the double layer, i.e., $E \sim \Delta\phi/2\kappa^{-1}$ but diminishes quickly towards the bulk. Such non-uniformity in electric field can be seen in **Figure 6** for several different salt concentrations. Therefore, particles in the bulk can always rotate freely because they experience very little electric torque and Brownian motions simply dominate, as we observed in experiments. Once particles approach the substrate, they start to feel the strong non-zero field, which can well exceed the applied field. The enhanced field is, however, only within ~1 μm from the electrode at low salt concentrations, which is about the size of one lobe in the dumbbell particles. As shown in the inset of Figure 6, the whole dimer feels the appreciable field when it lies on the substrate, while only half of it experiences the strong field when it stands. Therefore, dumbbells would like to assume lying orientations to minimize the induced-dipole-field interaction energy. At all salt concentrations, the appreciable DC field is always confined less than 1 μm - not strong enough to align our dimers perpendicular to the substrate. This is consistent with our observation that dumbbells always lie on the substrate under DC field.

Second, we observe that the aggregation of particles (for both dumbbells and spheres) under DC field becomes weaker as the salt concentration increases. Based on Equation 2, the equilibrium-charge electroosmotic flow is proportional to the *actual* electric field across the particles. At high salt concentrations, the majority of the particle feels essentially a zero field. Therefore, the electroosmotic flow is weak. In fact, no assembly is observed in 10^{-3} M KCl solution under DC field.

Third, we find the threshold voltage for DC assembly is ~2.4 V, which is independent of the spacing between two electrodes. This at first appears counter-intuitive because the apparent field strength becomes weaker as the spacing increases. Physically, it is, however, not surprising because most of the voltage drop occurs within the double layer and the field in bulk is essentially zero. A mathematical examination of Equation (8) also reveals that the electric field distribution near the electrode is independent of the separation between two electrodes H. For $z = -H + \delta$ (where $\delta \ll H$), it can be shown that $E(\omega \to 0) \sim (\Delta\phi/2\kappa^{-1})e^{-\kappa\delta}$. Therefore, as long as the applied voltage and salt concentration are constant, varying the spacing between two electrodes does not affect the actual field distribution near the electrode, which in turn does not affect the aggregation behavior of particles. This reconciles the observation in previous DC-field assembly literature that the required voltage is on the same order of magnitude but the spacing can vary across several orders of magnitude.[29,31]

Fourth, we also notice that image charges and image dipoles may appear on the other side of the conducting electrode when particles are close to the electrode. The attraction between dimer particles and their images could also make the lying orientation more favorable, which could be important especially when the salt concentration is low.

2.5.2. Assembly Under AC Field

The distribution of an AC field near the electrode depends on both frequency and salt concentration. **Figure 7**a shows the electric field in a 10^{-3} M KCl solution, the same experimental condition in Figure 4. Similar to the DC field, there exists a transition zone ($\sim \kappa^{-1}$) from the electrode where the field is enhanced. Different from the DC field, the AC field in bulk is non-zero. Its strength increases with increasing frequency until it approaches the applied field ($E/E_0 \sim 1$) at high frequencies. For example, as shown in Figure 7a, the bulk field at 10^3 Hz is only about 1/20 of the applied field strength, while it equals to the applied field strength at ~10^5 Hz. Such characteristics in AC field helps explain the phase diagrams in Figure 4 and Figure 5 both qualitatively and quantitatively.

First, we find the orientation of an individual dimer (either on the substrate or in the bulk) strongly depends on the frequency even if the applied field strength is constant. Dimers typically orient their long axes parallel to the applied field (i.e., in the standing orientation) beyond a frequency threshold ~10^3 Hz, as indicated by the grey square and circle ω_c in Figure 4 and the thin line separating L-L and L-S regimes in Figure 5. This critical frequency can be predicted by considering the competition between the field-dipole energy $U_{FD}(\omega)$ and the thermal energy kT:

$$U_{FD}/kT \sim 2\pi\varepsilon_0\varepsilon_s ab^2 \mathrm{Re}(K_{\parallel} - K_{\perp})E(\omega)^2/kT \geq 1 \quad (9)$$

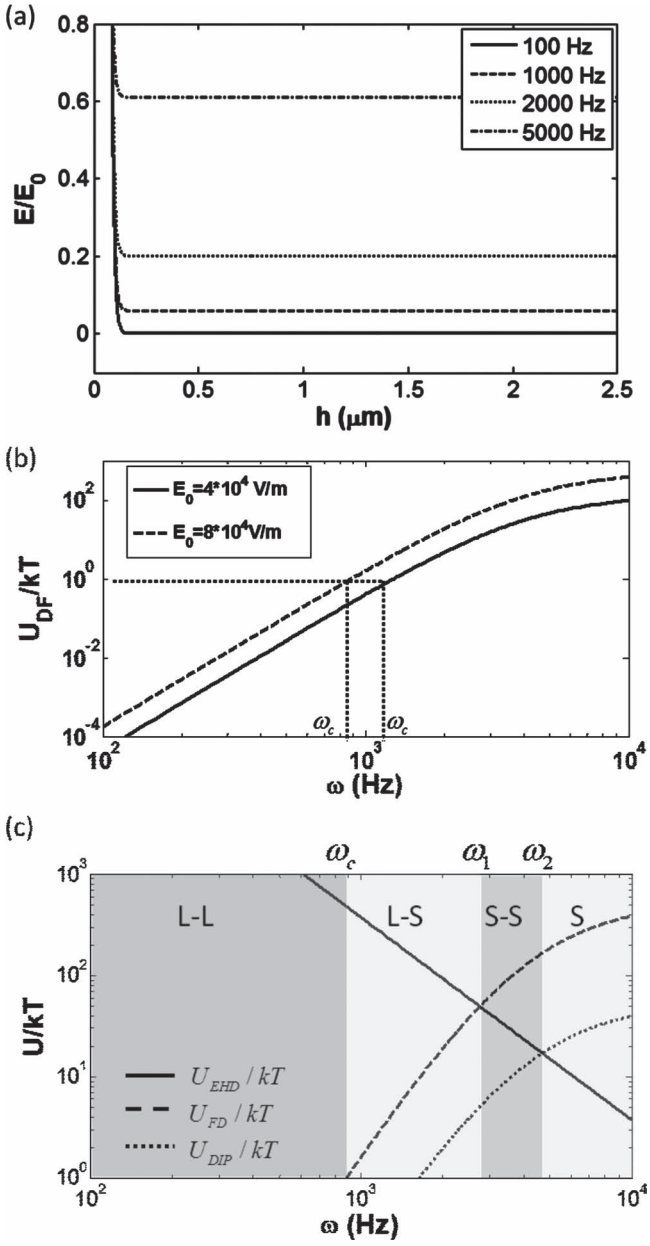

Figure 7. (a) AC field distribution at different frequencies in a constant salt concentration 10^{-3} M. h is the distance from the bottom electrode. (b) The field-dipole interaction energy U_{FD} at different frequencies. ω_c is the frequency at which $U_{FD} \sim kT$. (c) The plot of electro-hydrodynamic interaction U_{EHD}, dipolar interaction U_{DIP}, and field-dipole interaction U_{FD} at different frequencies. In the calculation, β is chosen 10^{-4} and the dipolar interaction is evaluated at $r = 2.5a$. Four different frequency regimes can be recognized: (1) L-L where $\omega < \omega_c$ and $U_{EHD} > 1 > U_{FD}$; (2) L-S where $\omega_c < \omega < \omega_1$ and $U_{EHD} > U_{FD} > U_{DIP}$; (3) S-S where $\omega_1 < \omega < \omega_2$ and $U_{FD} > U_{EHD} > U_{DIP}$; and (4) S where $\omega > \omega_2$ and $U_{FD} > U_{DIP} > U_{EHD}$.

Approximating the dumbbell with an ellipsoid and neglecting the concentration polarization, we obtain $\mathrm{Re}\left(K_{\parallel} - K_{\perp}\right) \sim 0.1$.[32] Plot of $U_{FD}(\omega)/kT$ is shown in Figure 7b for two different fields that were applied in Figure 4. From the graph, we find the critical frequency $\omega_c \sim 1300$ Hz for $E_0 = 4$V/100μm and ~800 Hz for $E_0 = 8$V/100μm. Both compare very well with our experimental measurement of $\omega_c \sim 1500$ Hz and ~900 Hz, as indicated by the grey square and circle in Figure 4.

Second, we hypothesize that the aggregation of dumbbells arises from the induced-charge electroosmotic flow (ICEO), the similar driving force for assembly of spherical particles. The particle velocity due to ICEO can be approximated as[34]

$$u_p = \beta u_{ICEO} \sim \beta \frac{3\varepsilon_0 \varepsilon_s}{2\mu\kappa} \left(\frac{\Delta\phi}{2H}\right)^2 \left[\mathrm{Re}\left(K_{\parallel(\perp)}\right)\left(1 + \frac{\kappa^3 D^2}{\omega^2 H}\right)\right] \quad (10)$$

where β is an empirical factor that relates the particle velocity to the ICEO solvent velocity. From Equation 10, we can further define a pseudo energy due to the ICEO (electro-hydrodynamic) interaction between particles:

$$U_{EHD}/kT \sim 6\pi\mu u_p a_{eff}^2/kT \quad (11)$$

where a_{eff} is the "effective" radius of the dumbbell. The force that balances the ICEO attraction would be the dipolar repulsion between dimers, whose interaction energy can be expressed as

$$U_{DIP}/kT = \frac{4\pi\varepsilon_0\varepsilon_s a^2 b^4 \mathrm{Re}\left(K_{\parallel(\perp)} K^*_{\parallel(\perp)}\right) E(\omega)^2}{kTr^3} \quad (12)$$

Here we neglect the double layer interaction since it is of extremely short range at high salt concentrations. Although not exactly the same, the hydrodynamic torque and the electric torque are on the similar order of magnitude with U_{EHD} and U_{DF}, respectively. The plots of U_{EHD}, U_{DIP}, and U_{FD} are shown in Figure 7c as functions of frequencies. When U_{EHD} is larger than U_{DIP} i.e., when $\omega < \omega_2$, particles experience a stronger attraction than repulsion so they aggregate. The aggregation regime can be further divided into three parts: (1) $\omega < \omega_c$: the electric toque is less than kT. Therefore, particles lie on the substrate during the assembly, corresponding to the L-L phase. (2) $\omega_c < \omega < \omega_1$: individual dumbbells stand on the electrode because $U_{FD} > 1$. The particles will still lie down when they approach the assembled structure because the hydrodynamic torque is larger than the electric torque, i.e., $U_{EHD} > U_{FD}$. Such effect can be clearly seen in the Supporting Information movie 4 for the L-S phase. (3) $\omega_1 < \omega < \omega_2$: the hydrodynamic torque is now smaller than the electric torque. Crystals of standing dimers (S-S) can then be obtained. Therefore, the competition between the hydrodynamic and electric torques determines the orientation of a particle during the process of assembly. When $\omega > \omega_2$: the aggregate disassembles because the electro-hydrodynamic attraction is weak ($\propto \omega^{-1}$ for spherical particles[30]) and is insufficient to balance the dipolar repulsion. In this regime, U_{FD} is much larger than kT. Therefore, the disassembled dumbbells adopt the standing orientation (S). Although the above order-of-magnitude estimation provides semi-quantitative agreement with experiments, we emphasize that the analysis is primitive. In particular, the anisotropic polarizabilities $K_{\parallel}$ and $K_{\parallel}$ are complex functions of frequency. The low frequency dependence of $K_{\parallel}$ and $K_{\parallel}$ has been neglected in our calculation because no simple model is available for dumbbells in literature currently. More quantitative comparison between theory and experiment is necessary but it is beyond the scope of this paper.

Third, it can be seen from Equation (9), Equation (11), and Equation (12) that U_{FD}, U_{EHD}, *and* U_{DIP} all depend on E^2_0.

Therefore, the phase diagram is qualitatively similar under different voltages. But they scale differently with the frequency, which is the main reason why rich phase behavior can be observed at different frequencies.

Last but not the least, the appearance of the "S-L" phase at very low frequency regime certainly deserves further study and might suggest that other mechanisms or forces can be involved. Supporting Information movie 2 suggests an attractive interaction between standing and lying dimers. We, however, do not have a confident explanation at this moment.

3. Conclusions

In this paper, we study two-dimensional assembly of symmetric colloidal dimers on a conducting substrate under the influence of electric fields. Different from spherical colloids, we observe rich phase behavior and aggregation modes primarily due to the geometric anisotropy in the dimer particles. By varying the frequency of the electric field, ramping direction of the frequency, and salt concentration, we demonstrate facile and precise control on both orientation and aggregation of colloidal dimers. Within the frequency range that we have explored, the electric torque favors alignment of dimers along the applied field, while the hydrodynamic torque tends to align particles perpendicularly. Brownian motions prevent perfect alignment in either direction. Therefore, the competition and delicate balance between the electric, hydrodynamic, and Brownian torques dictate the orientation of individual dimers in the bulk, on the substrate but far away from the aggregate, and within the aggregate. We also show that the conducting nature of the substrate plays a vital role. It generates the electro-hydrodynamic flow on the substrate, the main mechanism for attractive motion between dumbbells. Moreover, the non-uniform field distribution close to the conducting substrate is important to understand different frequency-dependent phenomena observed in our experiments. We have provided order of magnitude estimations that agree with experimental observations semi-quantitatively. From the practical perspective, we successfully make close-packed crystals of standing dimers, which is an important step towards 3D fabrication of photonic crystals based on dimer particles. From the scientific aspect, our study reveals the complex nature and potential power in field-driven assembly of anisotropic particles, forming a fundamental baseline towards understanding the assembly of more complex building blocks, such as colloidal dimers with both geometric and interfacial anisotropies. We are currently investigating along those lines.

4. Experimental Section

Synthesis of colloidal dimers: Synthesis of colloidal dimers is performed with a multiple-step seeded emulsion polymerization, based on an modification of Kim et al.[16] and Park et al.[18] In brief, spherical polystyrene particles (the seeds, ~1 μm) are first prepared by dispersion polymerization in a mixture of methanol and water.[41] The spherical particles are further cross-linked with styrene, divinylbenzene (DVB), and 3-(trimethoxysilyl) propylacrylate (TMSPA). In particular, a monomer solution, consisting of styrene (1 ml), DVB (50 μl), initiator 2,2′-Azobis(2.4-dimethyl valeronitrile) (0.02 g), and TMSPA (100 μl) is emulsified in a 4.5 ml aqueous solution of polyvinylpyrrolidone (PVP, 4.4% w/v) and sodium dodecyl sulfate (SDS, 0.22%) by ultrasonication for 10 minutes at the power of 20W. Seed particles (1 ml 10% w/v) are then mixed with this emulsion. The mixture is kept at room temperature for 12 hours to ensure full swelling of the seeds, followed by another 12-hour polymerization in a 75 °C oil bath. After polymerization, the crosslinked polystyrene spheres (CPS) are centrifuged and cleaned in de-ionized water for four times. Dimers are made via further swelling and polymerization of CPS with styrene. The procedure is similar to making CPS particles. First, a monomer solution, consisting of styrene, sodium styrene sulfonate, and initiator is emulsified in an aqueous mixture of PVP and SDS. After mixing the emulsion with CPS solutions, a second lobe (mainly consists of styrene monomers) grow on the original CPS particle. Further polymerization fixes the shape of colloidal dimers.

Characterization of the colloidal dimers: The morphologies and sizes of colloidal dimers are examined using SEM (JEOL JSM-7000F). The electrophoretic mobilities of particles in different salt (potassium chloride) concentrations are measured via a Zetasizer (Malvern ZEN 3600). Zeta potentials are then calculated from mobility measurements according to the methods suggested in literature.[42]

Electric field assembly: A thin film of dimer suspension is sandwiched between two parallel pieces of ITO glasses with insulating polymer film as the spacer. The spacer's thickness can be varied from 20 μm to 1 mm. ITO glasses are purchased from Sigma-Aldrich with surface resistivity of 15–25 Ω/sq. Before the experiment, ITO glasses are ultrasonically cleaned in acetone for 10 minutes and in isopropanol for another 10 minutes. After that the ITO glasses are exposed in oxygen plasma for 5 minutes to increase the amount of (negative) surface charges (since the colloidal dimers bear negative charges). DC or AC fields are applied between two ITO glasses by function generators (BK Precision 1698 and RTGOL DG 1022). Real time observations are performed on an inverted microscope (Olympus IX 71) and recorded with a CCD camera (Retiga 2000R).

Supporting Information

Supporting Information is available from the Wiley Online Library or from the author.

Acknowledgements

The authors would like to thank Kisun Yoon (Harvard) and Prof. David Weitz (Harvard) for help in initial synthesis of dimer particles. The authors also thank Prof. Joanna Aizenberg (Harvard), Dr. Guangnan Meng (Harvard), Christopher Wirth (CMU), Prof. Paul Sides (CMU), and Prof. David Wu (CSM) for insightful discussions.

Received: March 8, 2012
Revised: April 24, 2012
Published online: June 19, 2012

[1] S. C. Glotzer, M. J. Solomon, *Nat. Mater.* **2007**, *6*, 557.
[2] S. C. Glotzer, M. J. Solomon, N. A. Kotov, *AIChE J.* **2004**, *50*, 2978.
[3] A. B. Pawar, I. Kretzschmar, *Macromol. Rapid. Comm.* **2010**, *31*, 150.
[4] U. Banin, R. Costi, A. E. Saunders, *Angew. Chem. Int. Ed.* **2010**, *49*, 4878.
[5] D. Velegol, H. A. Jerri, J. J. Mcdermott, N. Chaturvedi, *AIChE J.* **2010**, *56*, 564.
[6] Y. Xia, B. Gates, Z.-Y. Li, *Adv. Mater.* **2001**, *13*, 409.
[7] I. D. Hosein, S. H. Lee, C. M. Liddell, *Adv. Funct. Mater.* **2010**, *20*, 3085.
[8] H. A. Atwater, A. Polman, *Nat. Mater.* **2010**, *9*, 205.
[9] S. J. Tan, M. J. Campolongo, D. Luo, W. L. Cheng, *Nat. Nanotechnol.* **2011**, *6*, 268.

[10] A. Perro, S. Reculusa, S. Ravaine, E. Bourgeat-Lami, E. Duguet, *J. Mater. Chem.* **2005**, *15*, 3745.
[11] S. Jiang, Q. Chen, M. Tripathy, E. Luijten, K. S. Schweizer, S. Granick, *Adv. Mater.* **2010**, *22*, 1060.
[12] J. P. Singh, P. P. Lele, F. Nettesheim, N. J. Wagner, E. M. Furst, *Phys. Rev. E.* **2009**, *79*, 050401.
[13] J. B. Rivest, S. L. Swisher, L. K. Fong, H. M. Zheng, A. P. Alivisatos, *ACS Nano* **2011**, *5*, 3811.
[14] V. N. Manoharan, M. T. Elsesser, D. J. Pine, *Science* **2003**, *301*, 483.
[15] H. R. Sheu, M. S. Elaasser, J. W. Vanderhoff, *J. Polym. Sci. Pol. Chem.* **1990**, *28*, 629.
[16] J. W. Kim, R. J. Larsen, D. A. Weitz, *J. Am. Chem. Soc.* **2006**, *128*, 14374.
[17] E. B. Mock, H. De Bruyn, H. B. S. Hawkett, R. G. Gilbert, C. F. Zukoski, *Langmuir* **2006**, *22*, 4037.
[18] J. G. Park, J. D. Forster, E. R. Dufresne, *J. Am. Chem. Soc.* **2010**, *132*, 5960.
[19] I. D. Hosein, M. Ghebrebrhan, J. D. Joannopoulos, C. M. Liddell, *Langmuir* **2010**, *26*, 2151.
[20] K. Liu, Z. H. Nie, N. N. Zhao, W. Li, M. Rubinstein, E. Kumacheva, *Science* **2010**, *329*, 197.
[21] Q. Chen, S. C. Bae, S. Granick, *Nature* **2011**, *469*, 381.
[22] J. Henzie, M. Grünwald, A. Widmer-Cooper, P. L. Geissler, P. Yang, *Nat. Mater.* **2012**, *11*, 131.
[23] S. Gangwal, O. J. Cayre, M. Z. Bazant, O. D. Velev, *Phys. Rev. Lett.* **2008**, *100*, 058302.
[24] I. Kretzschmar, J. H. Song, *Curr. Opin. Colloid Interface Sci.* **2011**, *16*, 84.
[25] A. F. Demirors, P. M. Johnson, C. M. Van Kats, A. Van Blaaderen, A. Imhof, *Langmuir* **2010**, *26*, 14466.
[26] J. D. Forster, J. G. Park, M. Mittal, H. Noh, C. F. Schreck, C. S. O'hern, H. Cao, E. M. Furst, E. R. Dufresne, *ACS Nano* **2011**, *5*, 6695.
[27] D. Zerrouki, J. Baudry, D. Pine, P. Chaikin, J. Bibette, **2008**, 455, 380.
[28] M. Trau, D. A. Saville, I. A. Aksay, *Science* **1996**, *272*, 706.
[29] M. Bohmer, *Langmuir* **1996**, *12*, 5747.
[30] W. D. Ristenpart, I. A. Aksay, D. A. Saville, *Phys. Rev. E.* **2004**, *69*, 021405.
[31] D. C. Prieve, P. J. Sides, C. L. Wirth, *Curr. Opin. Colloid Interface Sci.* **2010**, *15*, 160.
[32] T. B. Jones, *Electromechanics of Particles*, Cambridge University Press, **1995**.
[33] Y. Solomentsev, M. Bohmer, J. L. Anderson, *Langmuir* **1997**, *13*, 6058.
[34] W. D. Ristenpart, I. A. Aksay, D. A. Saville, *J. Fluid. Mech.* **2007**, *575*, 83.
[35] J. A. Fagan, P. J. Sides, P. C. Prieve, *Langmuir* **2002**, *18*, 7810.
[36] C. L. Wirth, R. M. Rock, P. J. Sides, D. C. Prieve, *Langmuir* **2011**, *27*, 9781.
[37] D. A. Saville, T. Bellini, V. Degiorgio, F. Mantegazza, *J. Chem. Phys.* **2000**, *113*, 6974.
[38] C. Grosse, A. V. Delgado, *Curr. Opin. Colloid Interface Sci.* **2010**, *15*, 145.
[39] K. Q. Zhang, X. Y. Liu, *J. Chem. Phys.* **2009**, *130*, 184901.
[40] A. D. Hollingsworth, D. A. Saville, *J. Colloid Interface Sci.* **2003**, *257*, 65.
[41] F. Zhang, L. Cao, W. T. Yang, *Macromol. Chem. Phys.* **2010**, *211*, 744.
[42] A. V. Delgado, E. Gonzalez-Caballero, R. J. Hunter, L. K. Koopal, J. Lyklema, *Pure. Appl. Chem.* **2005**, *77*, 1753.